Electronic Supplementary Material (ESI) for Energy & Environmental Science.

Supplemental info for:

Empowering Multicomponent Cathode Materials for Sodium Ion Batteries by Exploring Three-Dimensional Compositional Heterogeneities

Muhammad Mominur Rahman,[a] Yahong Xu,[b] Hao Cheng,[c] Qianli Shi,[a] Ronghui Kou,[d] Linqin Mu,[a] Qi Liu,[e] Sihao Xia,[b] Xianghui Xiao,[d] Cheng-Jun Sun,[d] Dimosthenis Sokaras,[b] Dennis Nordlund,[b] Jin-Cheng Zheng,[c] Yijin Liu,[b*] Feng Lin[a*]

a) Department of Chemistry, Virginia Tech, Blacksburg, VA, 24061, USA
b) Stanford Synchrotron Radiation Lightsource, SLAC National Accelerator Laboratory, Menlo Park, California 94025, USA
c) Department of Physics and the Collaborative Innovation Center for Optoelectronic Semiconductors and Efficient Devices, Xiamen University, Xiamen 361005, China; Xiamen University, Malaysia, 439000, Sepang, Selangor, Malaysia
d) Advanced Photon Source, Argonne National Laboratory, Argonne, Illinois 60439, USA
e) Department of Physics, City University of Hong Kong, Kowloon, Hong Kong

Corresponding authors: Y.L. liuyijin@slac.stanford.edu F.L. fenglin@vt.edu

Table S1. Overall elemental composition of all materials as determined by ICP-AES analysis.

Material	Na	Mn	Fe	Cu
CFM-Cu	0.882	0.527	0.279	0.194
CFM-Fe	0.939	0.518	0.276	0.207
CFM-Mn	0.938	0.507	0.291	0.203
CFM-H	0.921	0.517	0.285	0.198

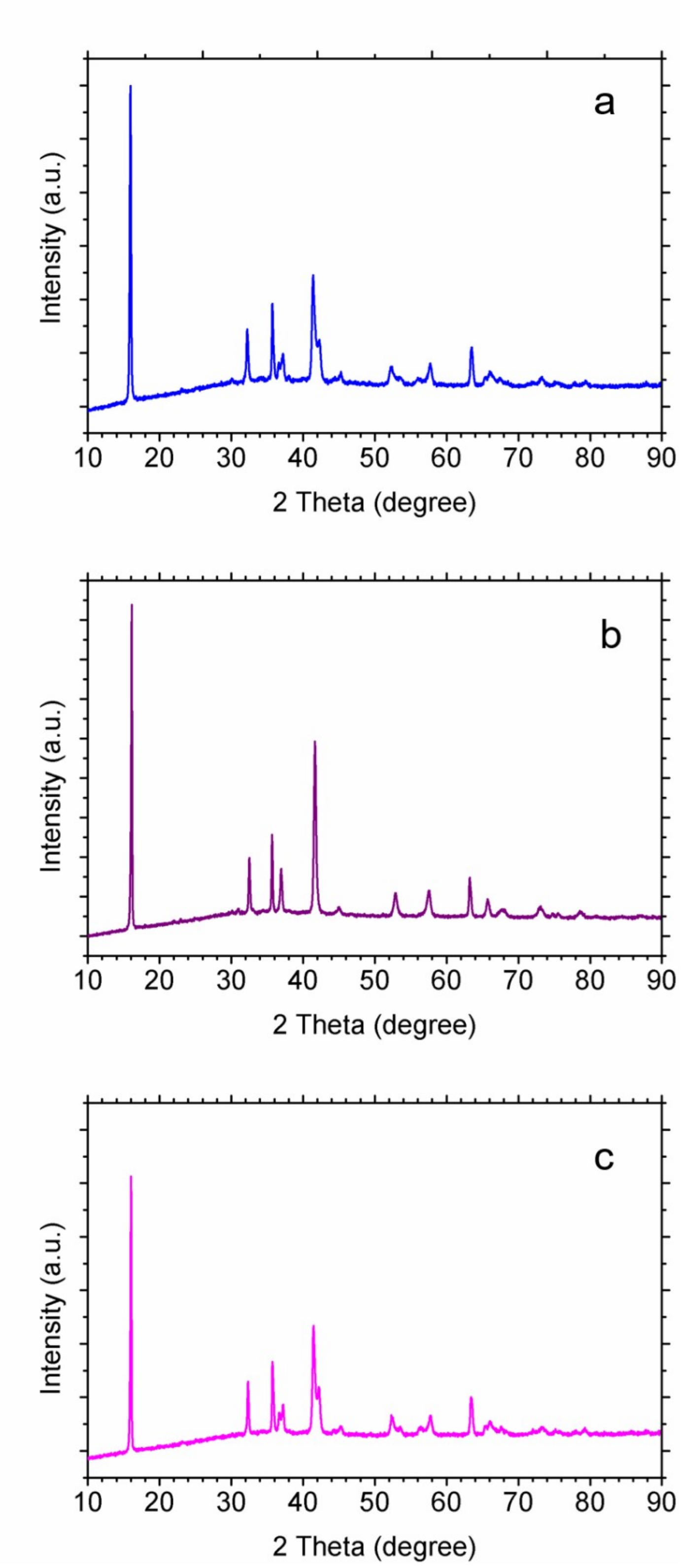

Figure S1. XRD pattern for the pristine powders of a) CFM-Fe, b) CFM-Mn and c) CFM-H

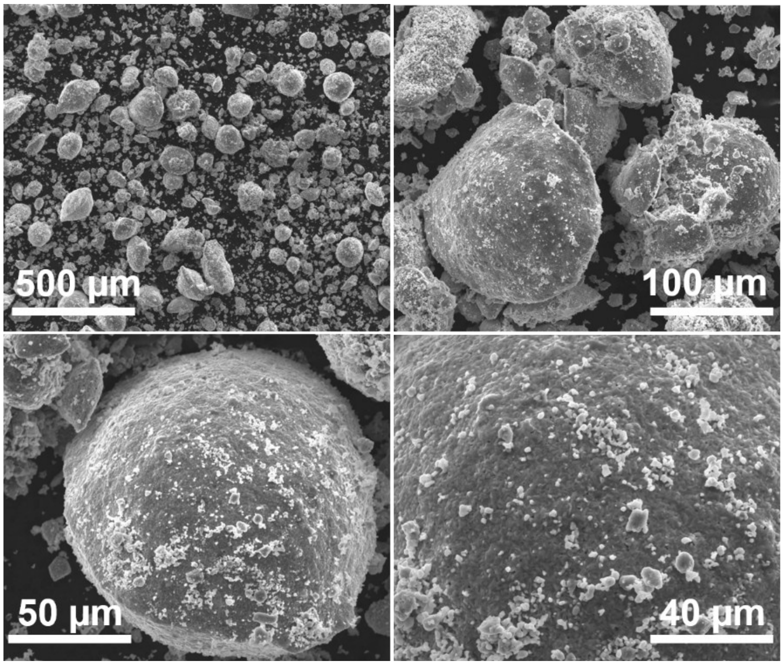

Figure S2. SEM micrographs of pristine powder of CFM-Fe

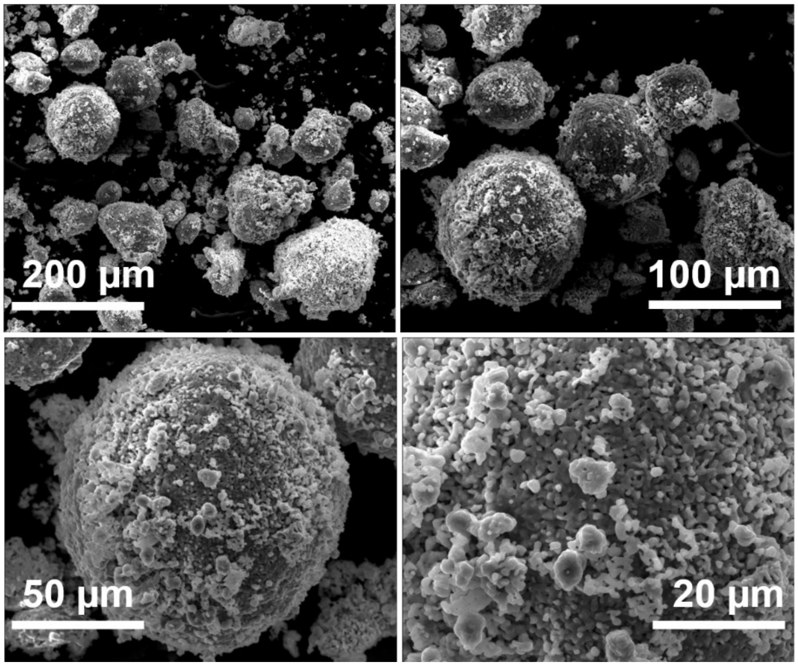

Figure S3. SEM micrographs of pristine powder of CFM-Mn

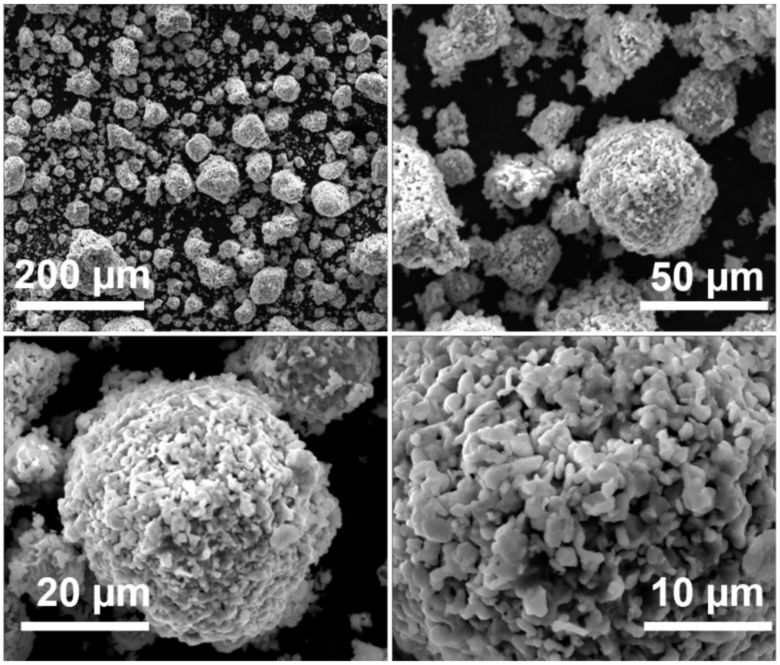

Figure S4. SEM micrographs of pristine powder of CFM-H

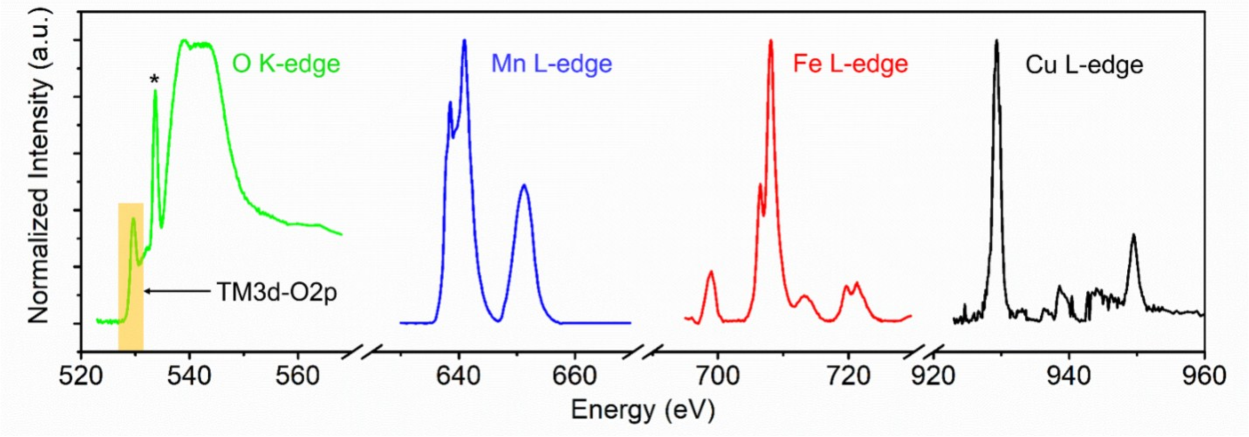

Figure S5: Soft XAS spectra of O K-edge (peak marked by "*" is due to O from surface carbonate species), Mn L-edge, Fe L-edge, and Cu L-edge of pristine CFM-Cu electrode.

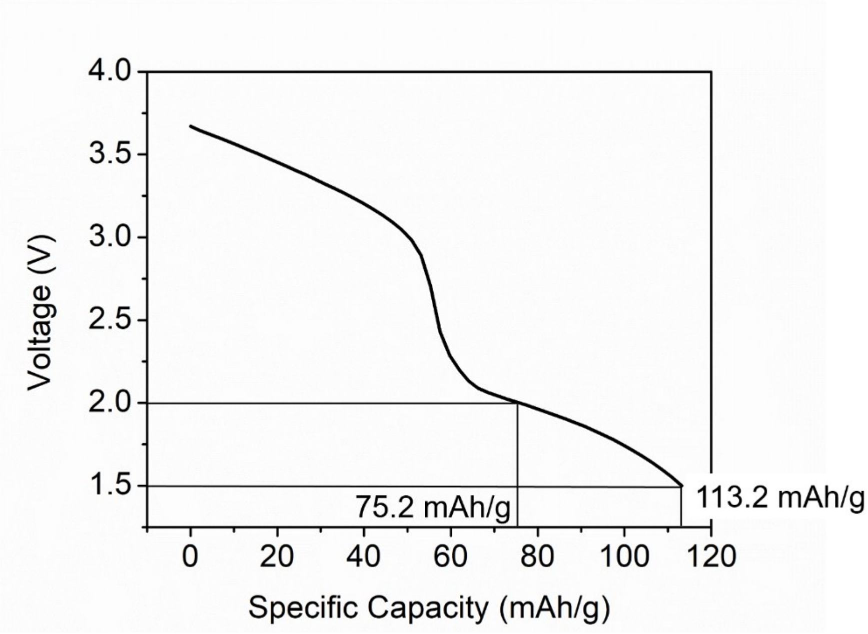

Figure S6. Discharge profile of CFM-Cu at 1C rate (voltage window 1.5-4.0V). The capacity was 75.2 mAh/g on discharging to 2.0V which corresponds to the capacity gained from the material on cycling between 2.0-4.0V window. However, on discharging to 1.5V, the capacity increased along with the extension of the low voltage plateau.

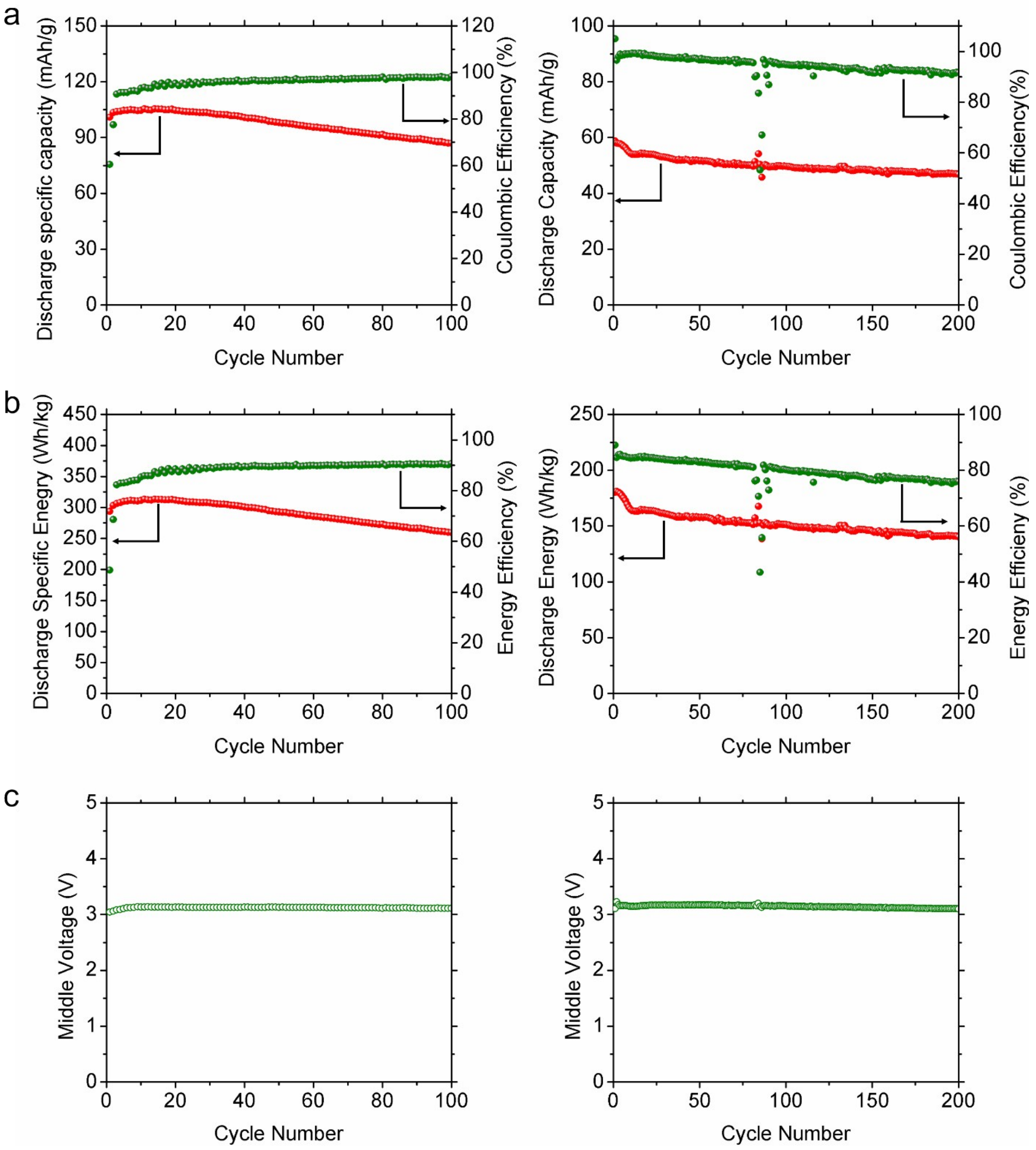

Figure S7. Electrochemical performance evaluation of CFM-Fe in a Na half-cells. (a) discharge specific capacity at C/10 and 1C charging rate, (b) discharge energy at C/10 and 1C charging rate and (c) middle voltage profile at C/10 and 1C rate.

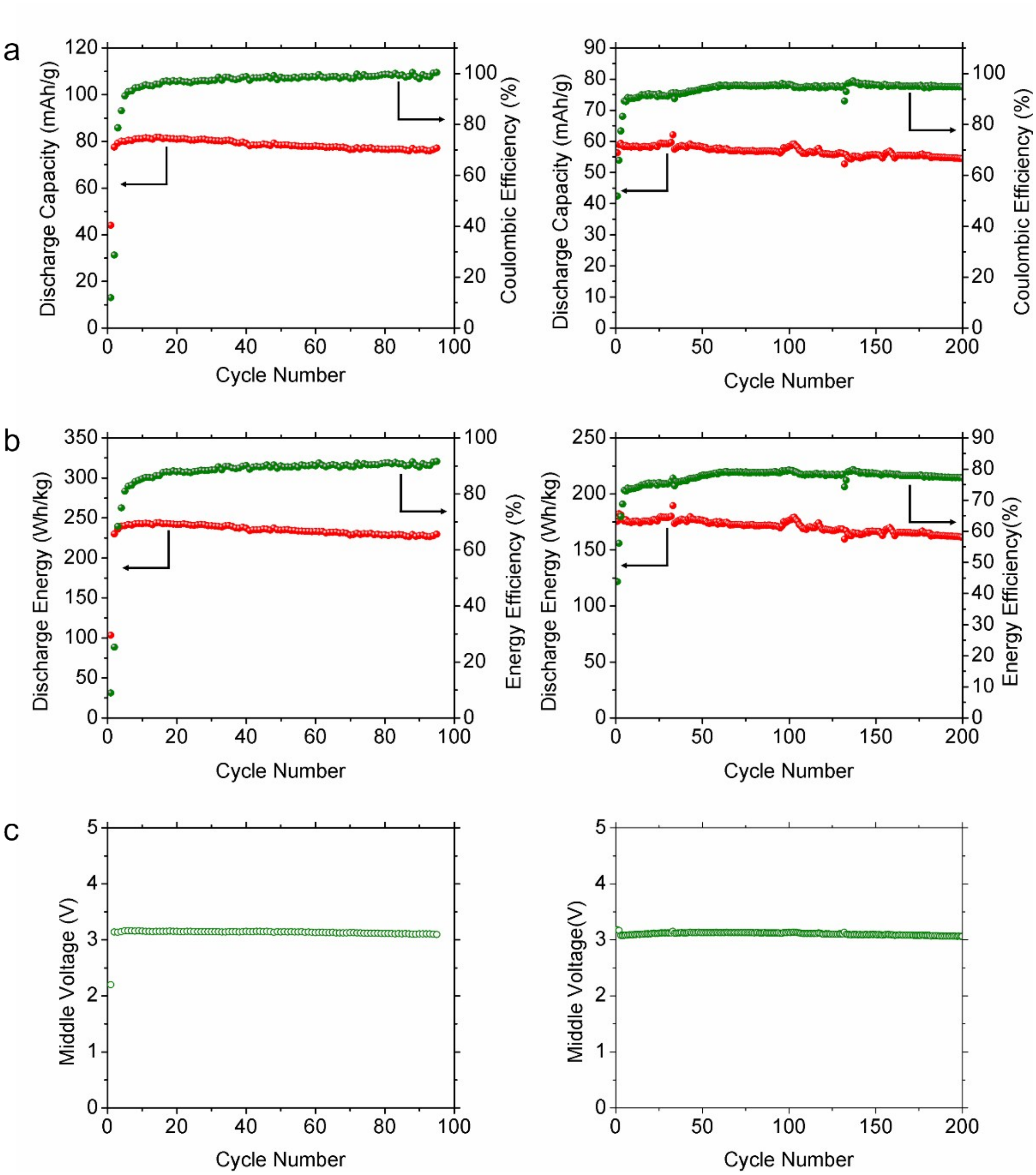

Figure S8. Electrochemical performance evaluation of CFM-Mn. (a) discharge specific capacity at C/10 and 1C charging rate, (b) discharge energy at C/10 and 1C charging rate and (c) middle voltage profile at C/10 and 1C rate.

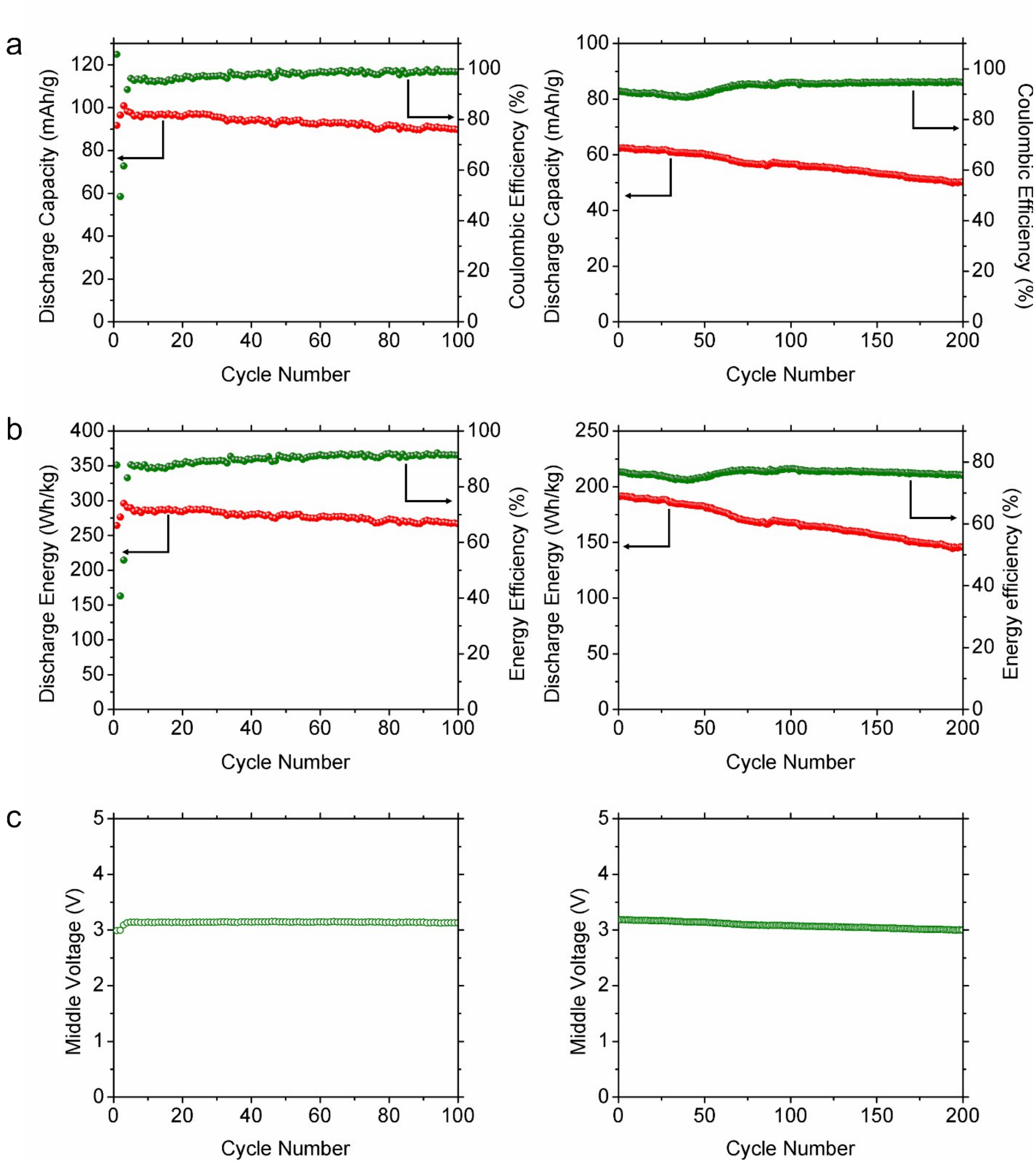

Figure S9. Electrochemical performance evaluation of CFM-H. (a) discharge specific capacity at C/10 and 1C charging rate, (b) discharge energy at C/10 and 1C charging rate and (c) middle voltage profile at C/10 and 1C rate.

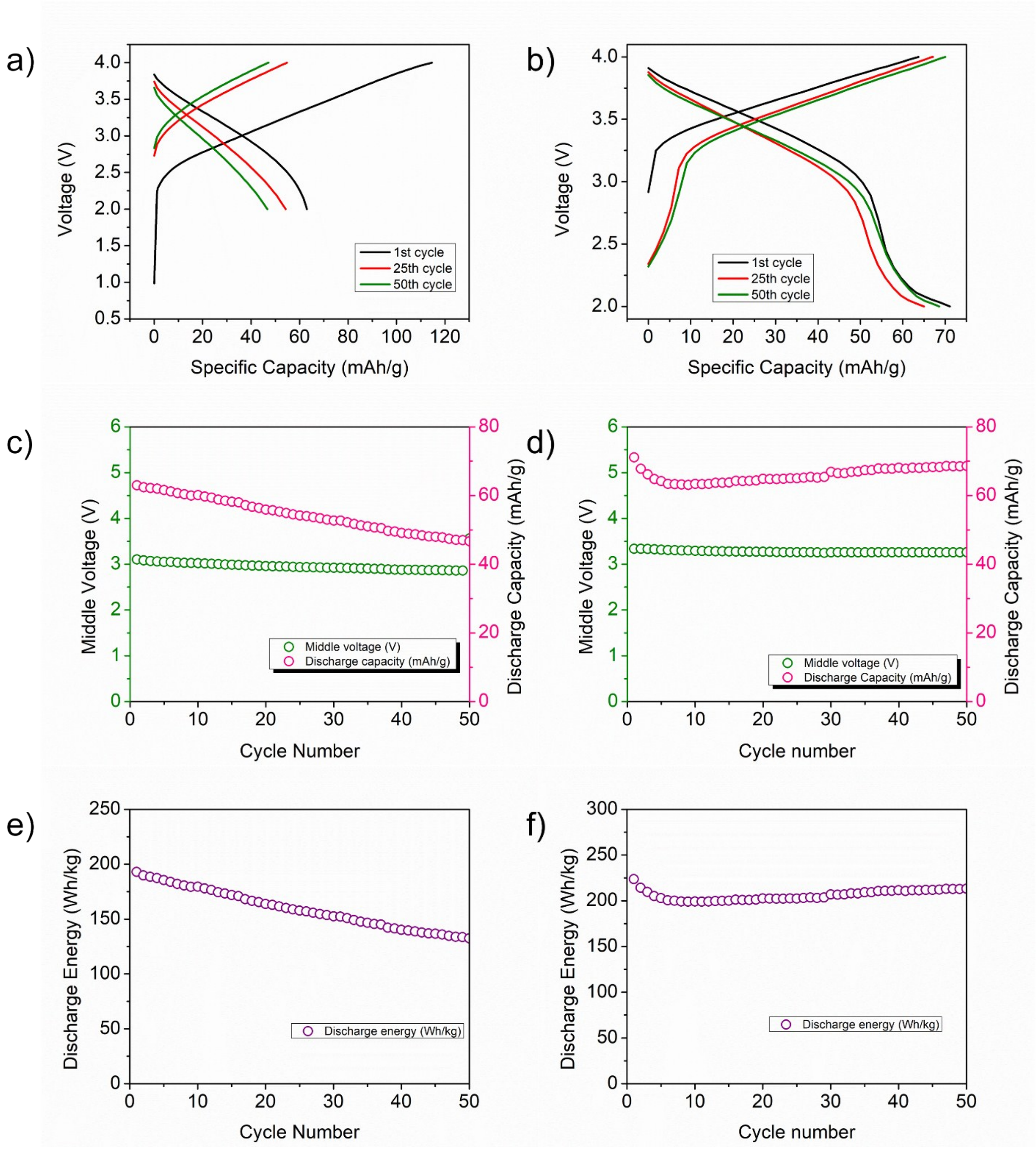

Figure S10. Electrochemical performance of CFM-Cu in a full cell with bare hard carbon and presodiated hard carbon anode at 1C rate. a) charge-discharge profile, c) middle voltage (V) and specific capacity (mAh/g) and e) discharge energy (Wh/kg) of the full cell with bare hard carbon. b) charge-discharge profile, d) middle voltage (V) and discharge capacity (mAh/g) and f) discharge energy (Wh/kg) oderived from the full cycle with prsodiated hard carbon.

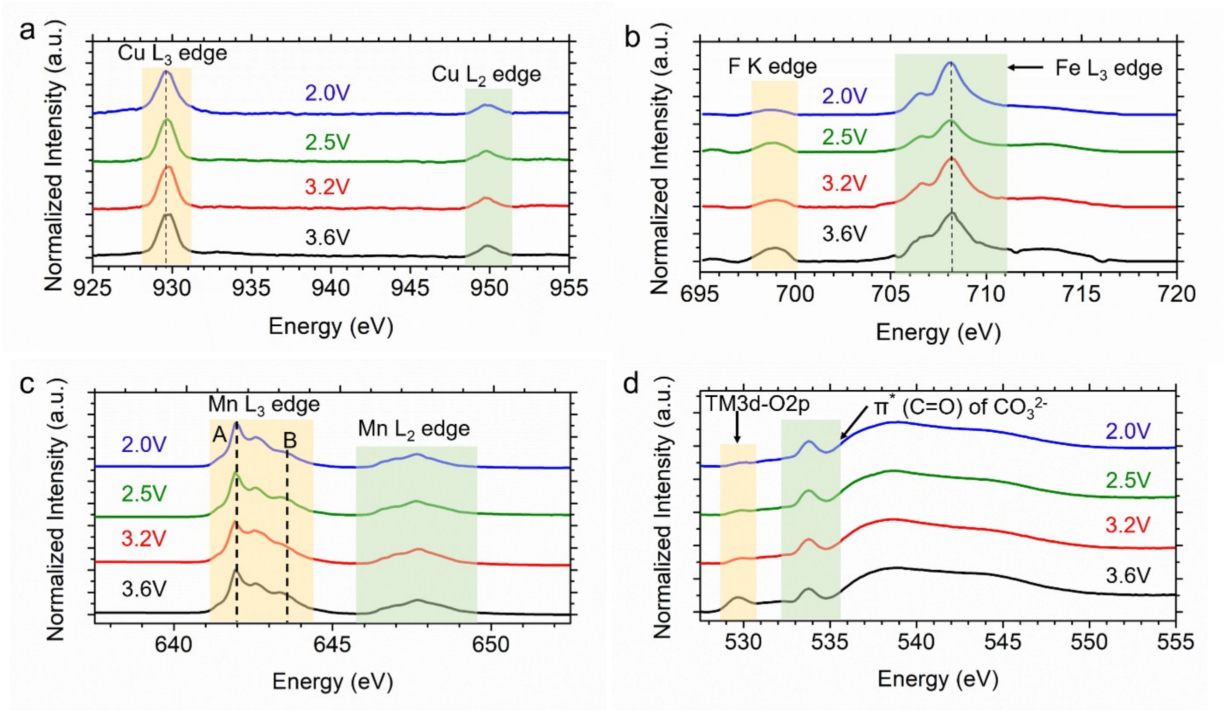

Figure S11. Surface sensitive soft XAS spectra (TEY mode) of CFM-Cu for (a) Cu L-edge, (b) Fe L-edge, (c) Mn L-edge, peaks labelled as A and B gradually changed in intensity as a function of discharge and (d) O K-edge at different states of charge in the first discharge cycle at C/10 rate. Color scheme: black spectra: discharged to 3.6V, red spectra: discharged to 3.2V, green spectra: discharged to 2.5V and blue spectra: discharged to 2.0V.

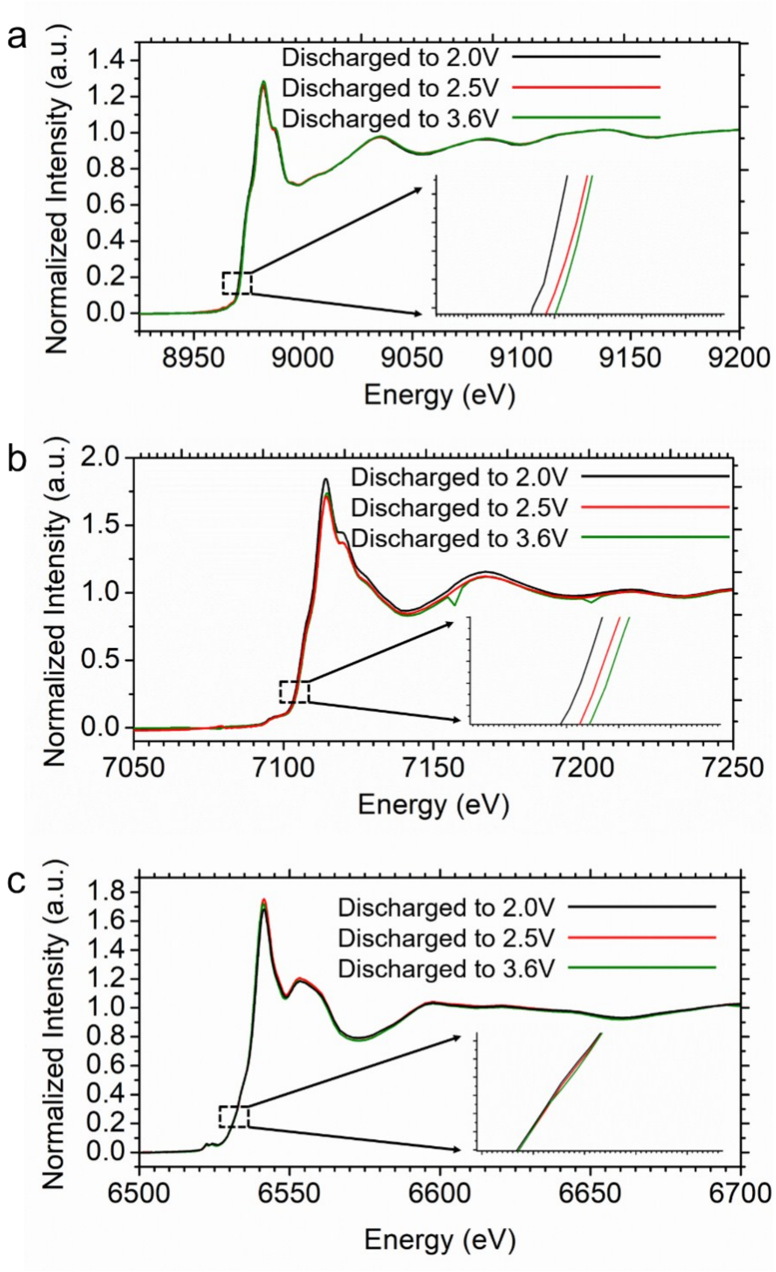

Figure S12. Hard XAS spectra of CFM-Cu for (a) Cu K-edge, (b) Fe K-edge and (c) Mn K-edge at different states of charge during the first discharge cycle at C/10 rate. The inset shows the zoom-in of the boxed portion of the spectra.

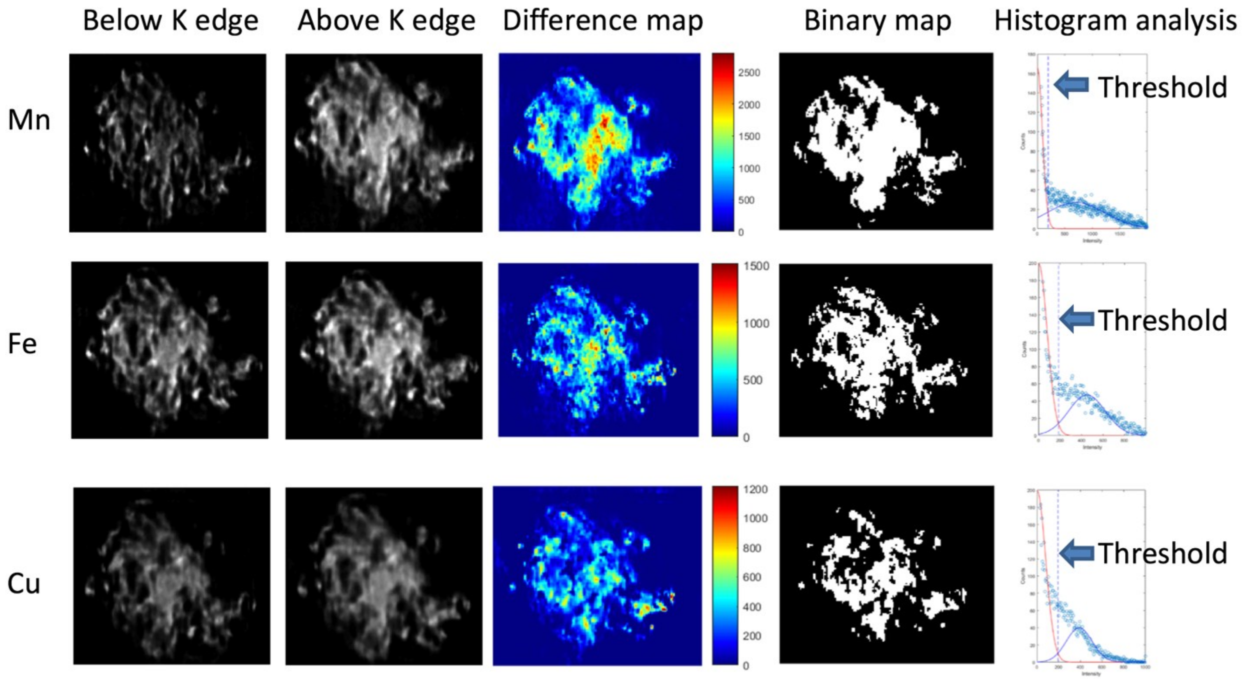

Figure S13. Representative slices through the center of the secondary particle. The transmission images below and above the absorption K edges of the TMs are shown in column 1 and 2, respectively. Column 3 shows the difference map, which represents the elemental distribution over the corresponding slice. Column 4 show the binary elemental maps, which are based on the threshold determined by the analysis of the histograms shown in column 5.

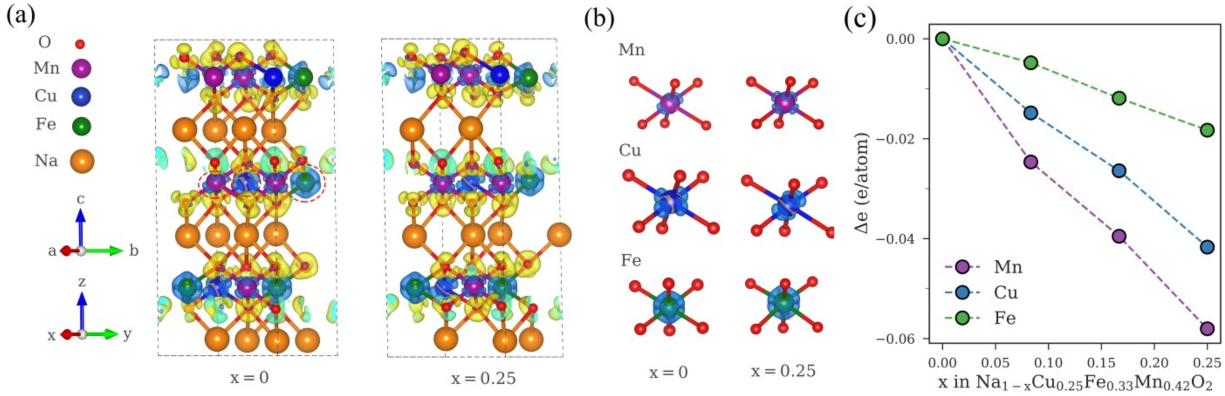

Figure S14. (a) The supercell crystal structure and difference charge density mapping for x=0 and x=0.25 in $Na_{1-x}Cu_{0.25}Fe_{0.33}Mn_{0.42}O_2$ respectively. The colored spheres indicate red for oxygen, purple for Mn, blue for Cu, green for Fe, and yellow for Na. The colored bands represent charge depletion for blue bands, charge accumulation for yellow bands and cyan for cross sections of the bands with the simulation box. The transitional metal atoms with most significance charge density change are pointed with red dashed cycle in (a) and are individually plotted with the nearest atoms in (b). (c) The average transfer charge on Fe, Cu, and Mn in $Na_{1-x}Cu_{0.25}Fe_{0.33}Mn_{0.42}O_2$, as a function of composition x, predicted by Bader analysis. The colored dots are purple for manganese, blue for copper, and green for iron, respectively.

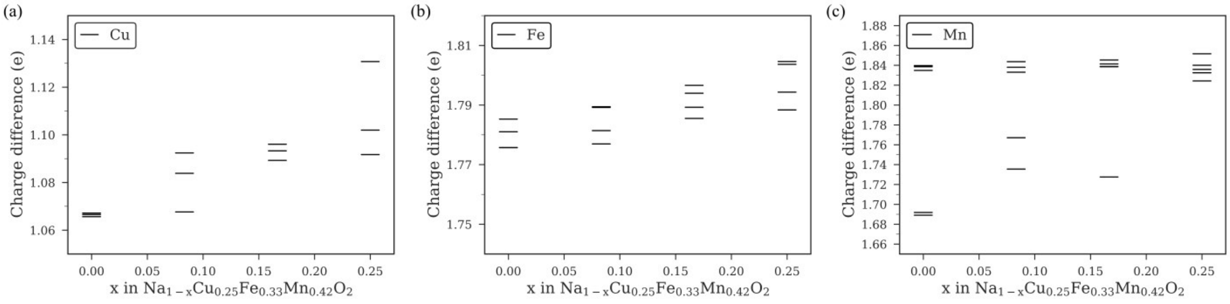

Figure S15. Bader charge analysis of transition metal (a) Cu, (b) Fe, and (c) Mn at different sites in $Na_{1-x}Cu_{0.25}Fe_{0.33}Mn_{0.42}O_2$.

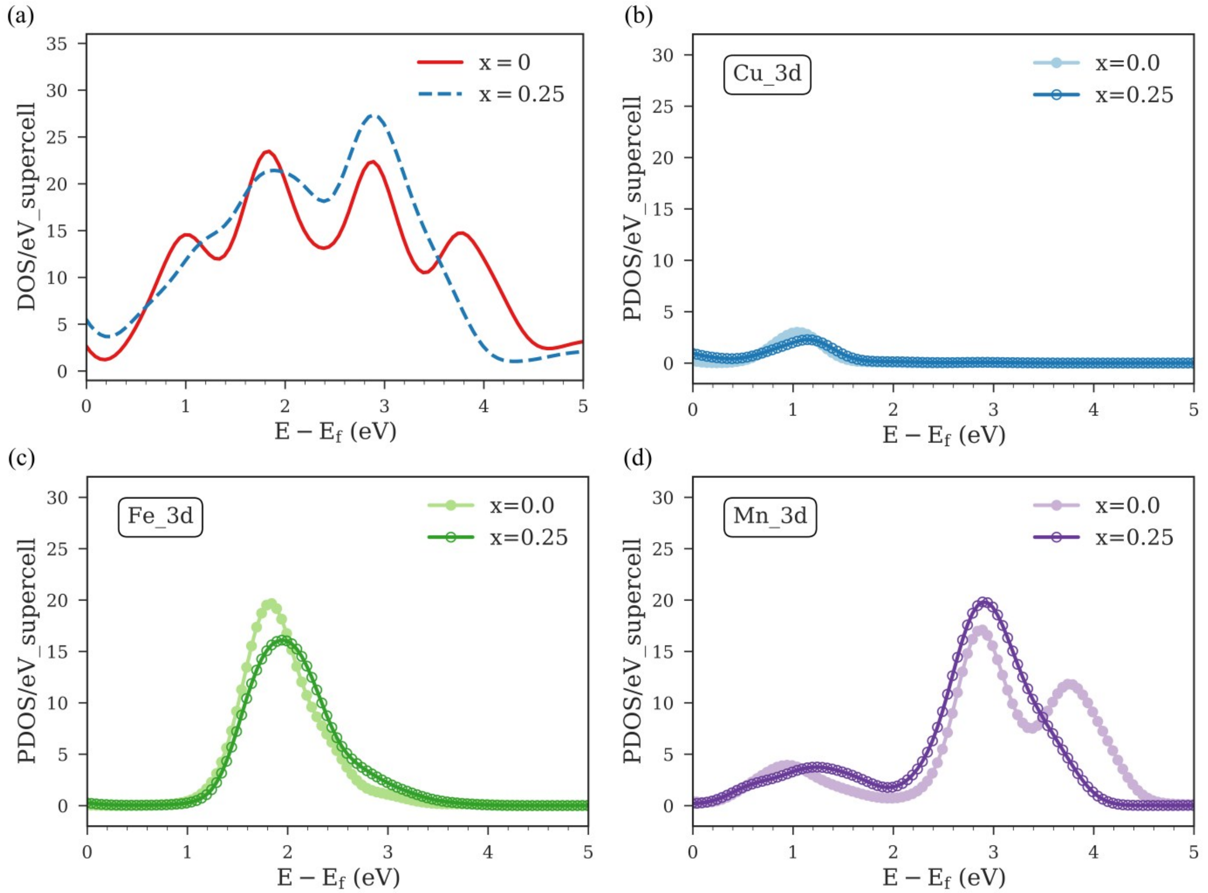

Figure S16. The Density of State (DOS) and Partial Density of State (PDOS) for x = 0 and x = 0.25 in Na$_{1-x}$Cu$_{0.25}$Fe$_{0.33}$Mn$_{0.42}$O$_2$.

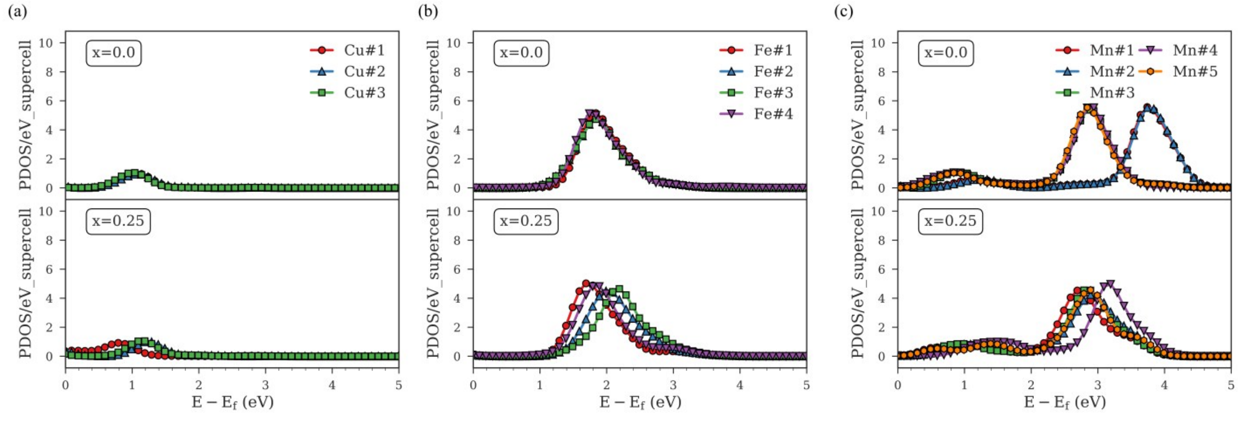

Figure S17. The PDOS of 3d electron orbital for each transition metal Cu (a), Fe(b), Mn(c) as x = 0 (upper panel) and x = 0.25 (lower panel) in Na$_{1-x}$Cu$_{0.25}$Fe$_{0.33}$Mn$_{0.42}$O$_2$.